

# Alignment of graphene oxide nanostructures between microgap electrodes *via* dielectrophoresis for hydrogen gas sensing applications

Budhi Singh, Jianwei Wang, Servin Rathi, and Gil-Ho Kim<sup>a)</sup>

School of Electrical and Electrical Engineering and Sungkyunkwan Advanced Institute of Nanotechnology (SAINT), Sungkyunkwan University, Suwon 440-746, South Korea

(Received 30 January 2015; accepted 12 May 2015; published online 20 May 2015)

Graphene oxide (GO) nanostructures have been aligned between conducting electrodes *via* dielectrophoresis (DEP) with different electrical configurations. The arrangement of ground with respect to peak-to-peak voltage ( $V_{pp}$ ) plays a crucial role in manipulating the GO nanostructures. Grounds on both sides of the  $V_{pp}$  electrode give an excellent linking of GO nanostructures which is explained by scanning electron microscopy and current-voltage characteristics. A finite element method simulation explains the electric field and voltage variation profile during DEP process. The optimized aligned GO nanostructures are used as hydrogen gas sensor with a sensitivity of 6.0% for 800 ppm hydrogen gas. © 2015 AIP Publishing LLC. [<http://dx.doi.org/10.1063/1.4921524>]

Graphene oxide (GO) is a fascinating carbon nanostructure and has received strong interest for device applications due to its exceptional electrical and optical properties. Its superior flexibility, large surface-to-volume ratio, chemical stability, and biocompatibility render GO an excellent material for electronic device applications.<sup>1–8</sup> The presence of functional groups provides an opportunity to modify its chemical functionalities as well as its optoelectronic properties.<sup>9</sup> Fully oxidized GO can be considered as insulating, while partially oxidized GO can act as a semiconductor. The band gap of GO can be tuned by just varying the oxidation level.<sup>10–13</sup> However, the integration of GO into a device in a controlled and precise manner has been challenging. Methods such as (i) drop casting, (ii) rapid freezing by spraying, and (iii) dip coating from GO suspensions have been used to obtain isolated individual and multilayer sheets or thin films.<sup>14–17</sup> Here, we describe dielectrophoresis (DEP) technique that allows uniform and controlled alignment of nanoparticles, nanotubes, and biomaterials for nano-device applications.<sup>18–30</sup> DEP of GO nanostructures allows the controlled manipulation of GO nanostructure thin films with thickness ranging from a single monolayer to several layers over a large area with an excellent linking of the electrodes. The GO nanostructure was assembled into microgap electrodes by controlling the DEP parameters, such as the applied frequency, applied peak-to-peak voltage ( $V_{pp}$ ), and processing time.<sup>31</sup>

DEP refers to the motion of electrically polarizable particles in non-uniform electric field gradients. The magnitude and direction of the DEP force depend on the relative polarizability of the particles and of the surrounding medium and is expressed as,  $\vec{F} = 2\pi r^3 \epsilon_0 \epsilon_m \text{Re}[K(\omega)] \nabla E^2$ , where  $\epsilon_0$  and  $\epsilon_m$  are the permittivity of the free space and the surrounding medium, respectively,  $r$  is the particle radius,  $\nabla E$  and is the electric field gradient.  $\text{Re}[K(\omega)]$  is the real part of the Clausius-Mossotti factor defined as,  $\text{Re}[K(\omega)] = \frac{\epsilon_p^* - \epsilon_m^*}{\epsilon_p^* + 2\epsilon_m^*}$ , where  $\epsilon^*$  is the complex permittivity and subscripts  $p$  and  $m$  denote the

particles and the medium, respectively.<sup>32,33</sup> In this letter, we show that the arrangement of electrical configuration plays a significant role during the DEP of the GO nanostructures, i.e., the arrangement of ground with respect to  $V_{pp}$  (i.e., with no ground, one ground, and two grounds) and the aligned network of GO nanostructures between microgap electrodes has been further used for hydrogen gas sensing at room temperature.

Fig. 1 shows the schematic representation of the experimental setup used for DEP process. The functional generator (Tektronix AFG 3102) connected with an oscilloscope (Tektronix TDS3052C) is used to supply an ac voltage at a particular fixed frequency. The Ti/Au electrodes with 4  $\mu\text{m}$  gaps were fabricated on a  $\text{SiO}_2/\text{Si}$  substrate using photolithography and lift-off technique. Prior to DEP process, the chip with Ti/Au with numbering from 1 to 5 was passed through a cleaning process using acetone and ethanol and rinsed with de-ionized water. Afterwards, the chip was dried with nitrogen gas. The GO nanostructures were synthesized by a modified Hummers method as described by Wang *et al.*<sup>21,22</sup> After DEP processing, scanning electron microscopy (SEM) (JEOL, Model: JSM-7401F) was used to examine the DEP alignment of GO nanostructures between the micro gap electrodes. An X-ray diffraction (XRD) study was carried out using a PANalytical Xpert Pro with nickel-filtered  $\text{CuK}\alpha$  ( $\lambda = 1.54 \text{ \AA}$ ) radiation as the X-ray source. The

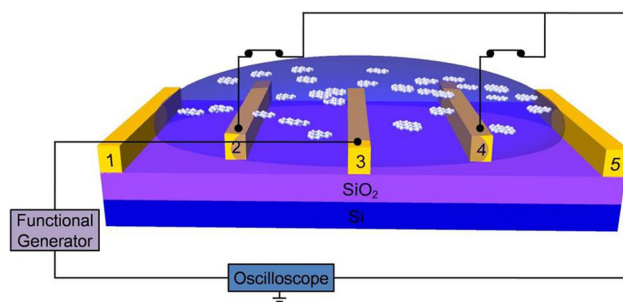


FIG. 1. Schematic representation of the setup used for the DEP of GO nanostructures. The Ti/Au electrodes with 4  $\mu\text{m}$  gap were fabricated on  $\text{SiO}_2/\text{Si}$  substrate with numbering from 1 to 5.

<sup>a)</sup> Author to whom correspondence should be addressed. Electronic mail: ghkim@skku.edu.

chemical bonding characteristics of the GO nanostructures were examined using X-ray photoelectron spectroscopy (XPS) (ESCA 2000, VG Microtech, UK) using twin anode X-ray sources  $K\alpha(1,486.6\text{ eV})/\text{Mg } K\alpha(1253.6\text{ eV})$  in a vacuum of  $10^{-9}$  Torr. A finite element method (FEM) was used to simulate the electric field profile of GO nanostructures on the Si/SiO<sub>2</sub> substrate. Current-voltage ( $I$ - $V$ ) characteristics of the assembled GO nanostructures were investigated using Keithley, Model: 4200-FCS  $I$ - $V$  measurement system. The sensing behavior of the assembled GO nanostructures device is performed in a vacuum chamber by observing the change in resistance with and without gas flow.

Fig. 2 shows the typical XPS data of the GO nanostructures with characteristic peaks of the  $sp^2$ -hybridized carbon, and hydroxyl, epoxy, and carboxyl functional groups. XRD pattern of the GO nanostructures with XRD peak at  $11.8^\circ$  is shown in the inset of Fig. 2. Similar XRD pattern correspond to 0.7 nm interlayer distance is observed by Wang et al.<sup>21,22</sup> During DEP, GO nanostructures with concentration of  $10\ \mu\text{g/ml}$  in de-ionized water is used because the spherical droplets with GO nanostructures inside can be readily generated between the electrodes. The relative permittivity of a GO nanostructure and water is 3 and 80, respectively, indicating  $\text{Re}[K(\omega)] > 0$  at DEP frequency less than  $10^{12}$  Hz.<sup>34,35</sup> This implies that GO nanostructures will be dragged to a region with higher electric field strength. A solution of GO ( $0.1\ \mu\text{l}$ ) was dripped into the Ti/Au electrode using a micropipette. A  $V_{pp}$  of 10 V with different ground at 500 kHz frequency was applied for 30 s to begin the DEP process. The  $V_{pp}$  of 10 V and 500 kHz frequency in 30 s duration are the optimized DEP parameters.<sup>22</sup> During DEP, the GO nanostructures are attracted randomly between the  $4\ \mu\text{m}$  gap electrodes and become immobilized before they are precisely aligned. After DEP processing, the sample was cleaned by isopropyl alcohol and gently dried by nitrogen flowing.

Fig. 3 shows the SEM images of the assembly of GO nanostructures between the micro gap electrodes when DEP was carried out at different ground configurations with respect to fixed  $V_{pp}$ . The darker region near the conducting electrode is the GO nanostructure aligned during DEP

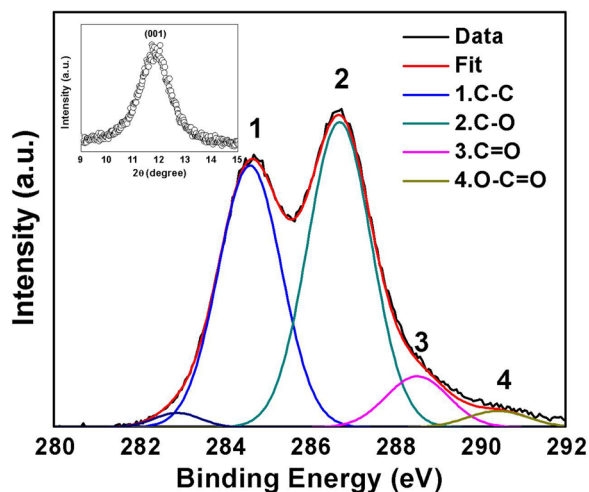


FIG. 2. XPS data of the GO nanostructures with characteristics peaks of  $sp^2$ -hybridized carbon, and hydroxyl, epoxy, and carboxyl functional groups. Inset shows the XRD pattern of the GO nanostructures.

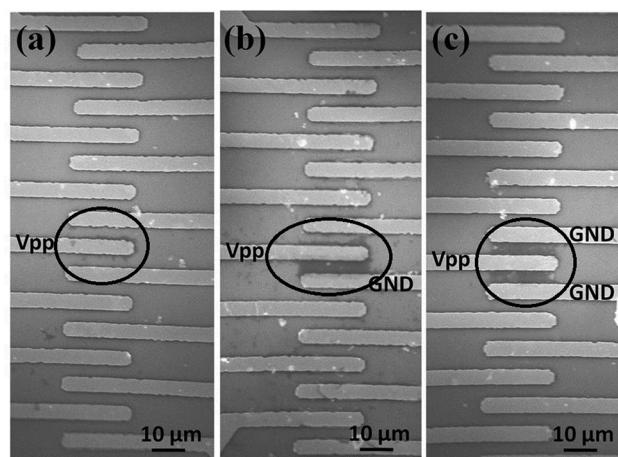


FIG. 3. SEM images of the GO nanostructures in Ti/Au electrodes when DEP was carried out using different electrical configurations of ground: (a) no ground, (b) single ground, and (c) double grounds with respect to  $V_{pp}$ . The darker region near the conducting electrode inside the circle is the GO nanostructure aligned during DEP process.

process. When DEP was carried out at  $10\ V_{pp}$  voltages with no ground at fixed 500 kHz and 30 s, it is found that the GO nanostructures are randomly distributed within the electrodes (Fig. 3(a)). This is because during DEP process no gradient field is developing within the electrodes that can align the GO nanostructures. Fig. 3(b) shows the SEM images of the GO nanostructure when DEP was carried out with one ground  $V_{pp}$ . From the SEM images, it is found that the GO nanostructure is well aligned at the ground side, while the GO nanostructures on the other part of the chip are not uniformly distributed. The density of the GO nanostructures decreases as we move away from the  $V_{pp}$  electrode, while there is no GO nanostructure present next to the ground electrode. This indicates that a ground with respect to  $V_{pp}$  provides sufficient field gradient to align the GO nanostructures between electrodes. When we use two grounds on both sides of the  $V_{pp}$  electrode, the alignment of the GO nanostructures is uniform as shown in Fig. 3(c) indicates excellent linking of GO nanostructures.

This precise alignment of the GO nanostructures can be further explained by FEM simulated electric field and voltage-profile of the GO nanostructures on Si/SiO<sub>2</sub> substrates. For simulation, a fixed  $V_{pp}$  was applied at one of the inner metal electrode using frequency domain mode set for 500 kHz. For the condition of single voltage source with no ground, a fixed potential of 10 V was applied at one electrode, while the ground was considered at an infinite point in the air surrounding the droplet. For other electrodes configuration, i.e., with single and double grounds, the condition for  $V_{pp}$  is similar but for the ground, zero electric potential was considered at the metal electrodes. The boundary conditions of current conservation and electric insulation were also applied to the enclosed simulated domain and SiO<sub>2</sub>, respectively. Fig. 4 shows the simulated electric field and voltage-profile inside the droplet with different electrical connections of (a) no ground, (b) one ground, and (c) two grounds, respectively. Simulation result shows that the electric field variation is not possible when there is no ground, and hence, there is no DEP force that can align the GO nanostructures

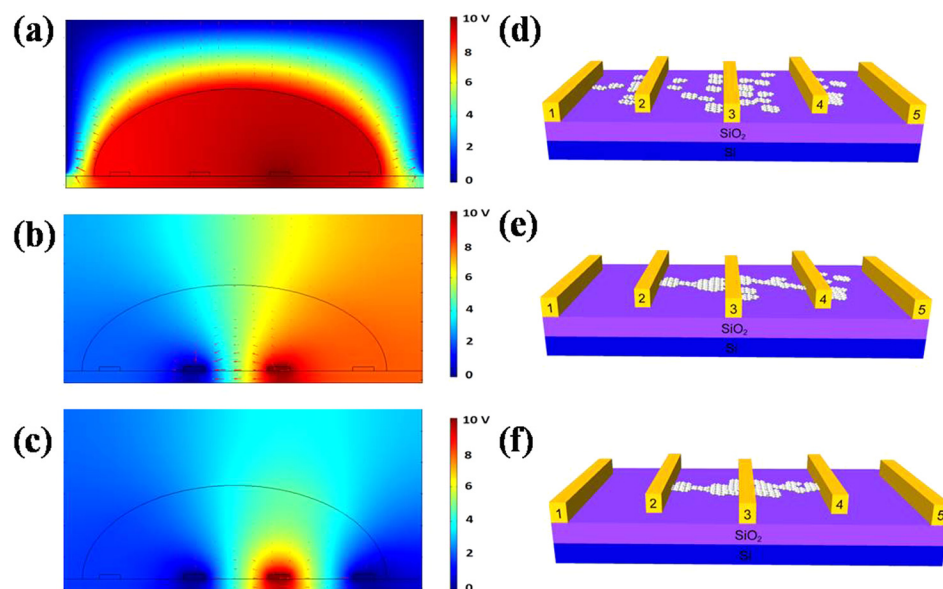


FIG. 4. (Left) FEM simulated electric field and voltage-variation indicated by arrow and color, respectively, between Ti/Au electrodes for different electrical configurations, (a) no ground, (b) single ground, and (c) double grounds with respect to  $V_{pp}$ . (Right) Schematic representation of the alignment of GO nanostructures between Ti/Au electrodes with (d) no ground, (e) single ground, and (f) double grounds.

between conducting electrodes. For no ground condition, we find that the electric field is negligible in the solution; however, it is stronger near the solution boundary in an upward direction (Fig. 4(a)). Hence, the probability for the alignment of GO nanostructures between Au electrodes is almost negligible. When we use one ground with respect to  $V_{pp}$  electrode, we observe that there is spatial distribution of electric field lines from the  $V_{pp}$  electrode towards the ground electrode (Fig. 4(b)). Due to this non-uniform electric field, an interfacial polarization between a GO nanostructure and water induces a  $F_{DEP}$  on the GO nanostructure. This induces  $F_{DEP}$  to align all the GO nanostructures from the ground side electrode in a precise manner, while the GO nanostructures are still randomly distributed on the other side of the  $V_{pp}$  electrode. This may be due to there being no electric field available to generate DEP force to align the GO nanostructure from the ground electrode side while a random electric field near the  $V_{pp}$  electrode results in GO accumulation on the other side. Therefore, when we use two grounds on both sides of the electrode, we find that all GO nanostructures align precisely between the electrodes. The schematic representation for the alignment of GO nanostructures between micro gap electrodes with different electrical configurations is shown in Figs. 4(d)–4(f), respectively.

The controlled manipulation of the GO nanostructures is further explained by  $I$ - $V$  measurement. Fig. 5(a) shows the  $I$ - $V$  characteristics of GO nanostructures when DEP process was carried out with no, single, and double grounds, respectively. It has been found that DEP process with no ground does not show any noticeable current. This indicates that no GO nanostructure channel formed between Au electrodes, clearly shown by the SEM images (Fig. 3(a)).  $I$ - $V$  characteristics with single and double grounds show linear behavior indicating a well aligned current path between Ti/Au electrodes. However, the  $I$ - $V$  behavior with two grounds shows an observed current value of one order of magnitude larger than the single ground value. This means that the DEP process with two grounds more prominently aligns the GO nanostructures with an excellent networking. The resistance value of the GO nanostructures is found to be 1 M $\Omega$  indicating the presence of the

functional groups as described by XPS analysis. The aligned GO nanostructures are further used for hydrogen gas sensing at 300 K. The resistance of the GO nanostructures decreases when exposed to hydrogen gas.<sup>13,21,36,37</sup> The adsorption kinetics of hydrogen gas on the surface of GO nanostructures is according to Langmuir kinetic theory which can be further modified by Freundlich isotherm considering that surface of GO nanostructure is inhomogeneous.<sup>38–41</sup> The gas sensitivity is defined as sensitivity =  $\frac{R-R_0}{R_0} \times 100\%$ , where  $R_0$  is the resistance when there is no target gas flow and  $R$  is the resistance with gas flow. Following steps are essential for sensing measurement, i.e., (i) clean air flow to record initial value of the resistance, (ii) the target gas with an optimized concentration has been introduced into a mixing chamber with clean air, (iii) flow of mixed gas to register a sensing signal, and (iv) clean air flow for sensing recovery. Fig. 5(b) shows the sensing behavior of the GO gas sensors fabricated with different electrical configurations when they are exposed to hydrogen gas at different concentrations from 200 ppm to 800 ppm, respectively. It has been found that the gas sensor formed with no ground shows almost zero response for hydrogen gas at all concentration because of the absence of GO network. On the other hand, the gas sensor with single and double ground configuration shows a sensitivity of  $\sim 1\%$  and  $\sim 4.0\%$ , respectively, for 200 ppm hydrogen gas. The large gas sensing response for double grounded configure device is expected as from SEM and  $I$ - $V$  characteristics. The sensitivity of the hydrogen gas for double ground configured device increases from  $\sim 4.0\%$  to  $\sim 6.0\%$  as the hydrogen gas concentration increases from 200 ppm to 800 ppm, respectively, whereas the sensitivity of hydrogen gas is almost constant for single ground configured device. This sensitivity is almost double when compared to the sensing devices fabricated *via* spin coated or drop casting method.<sup>13,22</sup> This is because the assembly of GO nanostructure between electrodes *via* spin coating or drop casting method requires a higher concentration of GO solution ( $\sim 1$ – $0.5$  mg/ml) to ensure electrical connection between the electrodes. This results in a comparatively thicker film of GO nanostructures which leads to reduced surface-to-volume ratio and hence the response of the sensing device

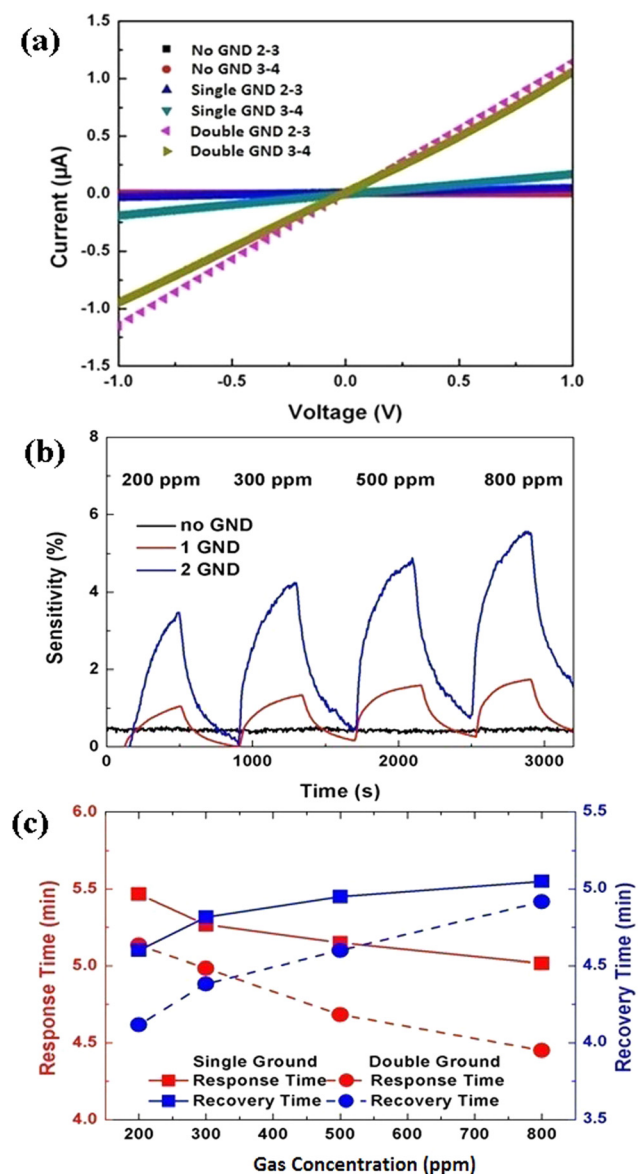


FIG. 5. (a) I-V characteristics of the GO nanostructures when DEP process was carried out with no ground, single ground, and double grounds with respect to  $V_{pp}$ . The No GND 2-3 or 3-4 means that the I-V characteristics between electrodes 2-3 or 3-4 and similar for other configurations. (b) Hydrogen gas sensing response of the GO sensors fabricated by DEP with different electrical configurations at different hydrogen gas concentrations from 200 ppm to 800 ppm, respectively. (c) Response and recovery time of the single and double ground configured GO nanostructures based gas sensor at different hydrogen gas concentrations.

decreases. On the other hand, an extremely low concentration of GO solution (0.1–0.01 mg/ml) is used for the DEP of GO nanostructures, which results in the increased surface-to-volume ratio as only few layers GO nanostructures are aligned under DEP forces instead of thick multi-layers.<sup>22</sup> Fig. 5(c) shows the response time and the recovery time of the GO gas sensors with single and double ground configuration at various hydrogen gas concentrations. The recovery time of the gas sensors increases whereas the response time decreases as the hydrogen gas concentration increases from 200 ppm to 800 ppm, respectively. Over all, the sensitivity, recovery time, and response time of the double grounded configure GO nanostructures based gas sensor at 800 ppm hydrogen gas are 6.0%, 306 s, and 270 s, respectively.

In conclusion, we aligned GO nanostructures between conducting electrodes by DEP method with different electrical configurations. It is found that the configuration of ground electrode with respect to  $V_{pp}$  electrode plays a crucial role in the alignment of GO nanostructures in a precise and controlled manner. Grounds on both sides of the  $V_{pp}$  electrode are essential for GO nanostructures manipulation, which is well explained by SEM images and I-V characteristics. The excellent alignment of GO nanostructures between conducting electrode *via* double grounded configuration is further explained by observing hydrogen gas sensing behavior of GO nanostructure at different gas concentrations and it has been found that the sensitivity, response time, and recovery time for 800 ppm hydrogen gas at 300 K are 6.0%, 270 s, and 306 s, respectively.

This research was supported by Basic Science Research Program through the National Research Foundation of Korea (NRF) funded by the Ministry of Education, Science and Technology (2013R1A2A2A01069023).

<sup>1</sup>D. S. Sutar, G. Singh, and V. D. Botcha, *Appl. Phys. Lett.* **101**, 103103 (2012).

<sup>2</sup>S. Saxena, T. A. Tyson, S. Shukla, E. Negusse, H. Chen, and J. Bai, *Appl. Phys. Lett.* **99**, 013104 (2011).

<sup>3</sup>H. W. Kim, H. W. Yoon, S. M. Yoon, B. M. Yoo, B. K. Ahn, Y. H. Cho, H. J. Shin, H. Yang, U. Paik, S. Kwon, J. Y. Choi, and H. B. Park, *Science* **342**, 91 (2013).

<sup>4</sup>R. Y. N. Gengler, D. S. Badali, D. Zhang, K. Dimos, K. Spyrou, D. Gournis, and R. J. D. Miller, *Nat. Commun.* **4**, 2560 (2013).

<sup>5</sup>K. Krishnamoorthy, R. Mohan, and S.-J. Kim, *Appl. Phys. Lett.* **98**, 244101 (2011).

<sup>6</sup>Q. He, S. Wu, S. Gao, X. Cao, Z. Yin, H. Li, P. Chen, and H. Zhang, *ACS Nano* **5**, 5038 (2011).

<sup>7</sup>G. Lu, S. Park, K. Yu, R. S. Ruoff, L. E. Ocola, D. Rosenmann, and J. Chen, *ACS Nano* **5**, 1154 (2011).

<sup>8</sup>G. Eda, G. Fanchini, and M. Chhowalla, *Nat. Nanotechnol.* **3**, 270 (2008).

<sup>9</sup>A. Allahabakhsh, F. Sharif, and S. Mazinani, *Nano* **8**, 1350045 (2013).

<sup>10</sup>T. S. Sreeprasad and V. Berry, *Small* **9**, 341 (2013).

<sup>11</sup>K. P. Loh, Q. Bao, G. Eda, and M. Chhowalla, *Nat. Chem.* **2**, 1015 (2010).

<sup>12</sup>Y. Zhu, X. Li, Q. Cai, Z. Sun, G. Casillas, M. J. Yacaman, R. Verduzco, and J. M. Tour, *J. Am. Chem. Soc.* **134**, 11774 (2012).

<sup>13</sup>J. Wang, K. Kwak, I.-Y. Lee, S. Maeng, and G. H. Kim, *Carbon* **50**, 4061 (2012).

<sup>14</sup>X. Wang, L. Zhi, and K. Mullen, *Nano Lett.* **8**, 323 (2008).

<sup>15</sup>H. C. Schniepp, J. L. Li, M. J. McAllister, H. Sai, M. H. Alonso, D. H. Adamson, R. K. Prud'homme, R. Car, D. A. Saville, and I. A. Aksay, *J. Phys. Chem. B* **110**, 8535 (2006).

<sup>16</sup>S. Gilje, S. Han, M. Wang, K. L. Wang, and R. B. Kaner, *Nano Lett.* **7**, 3394 (2007).

<sup>17</sup>C. Gómez-Navarro, R. T. Weitz, A. M. Bittner, M. Scolari, A. Mews, M. Burghard, and K. Kern, *Nano Lett.* **7**, 3499 (2007).

<sup>18</sup>Y. Demircan, E. Ozgur, and H. Kulah, *Electrophoresis* **34**, 1008 (2013).

<sup>19</sup>R. M. Duarte, *Electrophoresis* **33**, 3110 (2012).

<sup>20</sup>S. Kumar, Y. K. Seo, and G. H. Kim, *Appl. Phys. Lett.* **94**, 153104 (2009).

<sup>21</sup>J. Wang, B. Singh, S. Maeng, H. I. Joh, and G. H. Kim, *Appl. Phys. Lett.* **103**, 083112 (2013).

<sup>22</sup>J. Wang, B. Singh, J. Park, S. Rath, I. Lee, S. Maeng, H. I. Joh, C. H. Lee, and G. H. Kim, *Sens. Actuators, B* **194**, 296 (2014).

<sup>23</sup>D. Cheon, S. Kumar, and G. H. Kim, *Appl. Phys. Lett.* **96**, 013101 (2010).

<sup>24</sup>K. D. Hermanson, S. O. Lumsdon, J. P. Williams, E. W. Kaler, and O. D. Velev, *Science* **294**, 1082 (2001).

<sup>25</sup>H. A. Pohl and I. Hawk, *Science* **152**, 647 (1966).

<sup>26</sup>C. Chung, M. Waterfall, S. Pells, A. Menachery, S. Smith, and R. Pethig, *J. Electr. Bioimp.* **2**, 64 (2011).

<sup>27</sup>Y. Hwang, H. Sohn, A. Phan, O. M. Yaghi, and R. N. Candler, *Nano Lett.* **13**, 5271 (2013).

<sup>28</sup>H. A. Pohl, *J. Appl. Phys.* **22**, 869 (1951).

<sup>29</sup>L. Zheng, S. Li, J. P. Brody, and P. J. Burke, *Langmuir* **20**, 8612 (2004).

- <sup>30</sup>X. Q. Chen, T. Saito, H. Yamada, and K. Matsushige, *Appl. Phys. Lett.* **78**, 3714 (2001).
- <sup>31</sup>W. Li, X. Geng, Y. Guo, J. Rong, Y. Gong, L. Wu, X. Zhang, P. Li, J. Xu, G. Cheng, M. Sun, and L. Liu, *ACS Nano* **5**, 6955 (2011).
- <sup>32</sup>B. C. Gierhart, D. G. Howitt, S. J. Chen, R. L. Smith, and S. D. Collins, *Langmuir* **23**, 12450 (2007).
- <sup>33</sup>P. R. C. Gascoyne and J. Vykoukal, *Electrophoresis* **23**, 1973 (2002).
- <sup>34</sup>S. Pei, J. Zhao, J. Du, W. Ren, and H.-M. Cheng, *Carbon* **48**, 4466 (2010).
- <sup>35</sup>T. S. Bui, J. Kim, E. Jung, H. S. Le, N. T. Nguyen, and J.-Y. Bae, *Displays* **34**, 192 (2013).
- <sup>36</sup>V. C. Tung, M. J. Allen, Y. Yang, and R. B. Kaner, *Nat. Nanotechnol.* **4**, 25 (2009).
- <sup>37</sup>D. J. Late, A. Ghosh, K. S. Subrahmanyam, L. S. Panchakarla, S. B. Krupanidhi, and C. N. R. Rao, *Solid State Commun.* **150**, 734 (2010).
- <sup>38</sup>M. J. Madou and S. R. Morrison, *Chemical Sensing with Solid State Devices* (Academic, Boston, 1988).
- <sup>39</sup>L. Y. Kupriyanov, *Handbook of Sensors and Actuators, Semiconductor Sensors in Physico-Chemical Studies* (Elsevier, Amsterdam, 1996), Vol. 4.
- <sup>40</sup>M. Gautam and A. Jayatissa, *J. Appl. Phys.* **111**, 094317 (2012).
- <sup>41</sup>M. Gautam and A. Jayatissa, *J. Appl. Phys.* **112**, 064304 (2012).